

MATHEMATICAL MODELS AND SIMULATIONS OF
RECONFIGURABLE FLOW NETWORKS: EROSION,
DEPOSITION, FILTRATION AND GROWTH

Yuwei Bao, Tulane University, ybao2@tulane.edu

Isaac Castro, University of Texas at San Antonio, tbl707@my.utsa.edu

Gess Iraj, Brandeis University, gessiraji@brandeis.edu

Hamad El Kahza, New York Institute of Technology, helkahza@nyit.edu

Carlos Rojas Mena, University of Rochester, crojas3@ur.rochester.edu

Kiana Naghibzadeh, Carnegie Mellon University, snaghibz@andrew.cmu.edu

Andrea Weaver, University of Delaware, aweavs@udel.edu

Onyekachi Williams, Delaware State University, obwilliams19@students.desu.edu

Pejman Sanaei, New York Institute of Technology, psanaei@nyit.edu

GRADUATE STUDENT MATHEMATICAL MODELING CAMP (GSMMC)

UNIVERSITY OF DELAWARE, JUNE 2021

Abstract

Erosion, deposition, filtration and cell growth (EDFG) may seem unrelated at first, but they all stem from a set of similar first principles. These concepts show up in several different industrial applications such as: (i) petroleum geology for discovering natural gases or other natural resources trapped within the rocks; (ii) membrane filters, which are used in various critical aspects of human life such as water purification, the biotechnology industry, and kidney dialysis; and (iii) tissue engineering, which is vital in creating functional tissue and organ samples external to the body to replace damaged or diseased tissues and organs needed in multiple clinical therapies. In dynamic flow networks, reconfiguration and changes of topology that may arise due to EDFG, are very complicated processes, which are also expensive and challenging to study in most real-world applications. This workshop takes an integrated approach, to formulate (i) Stokes; (ii) advection-diffusion; and (iii) Navier-Cauchy equations for the flow, particle concentration and elasticity of complex structures, respectively. It is notable that the experimental literature far outweighs the theoretical and numerical literature; and among them there is a paucity of studies that offer first-principles, predictive mathematical models and simulations. The discoveries of this field have potential for significant impact in bridging this gap.

Contents

1	Introduction	5
2	Flow in a Channel	11
2.1	Governing Equations	11
2.2	Scaling and Non-Dimensionalization	14
2.3	Asymptotic Analysis	15
2.3.1	Leading-Order Analysis	16
2.3.2	First-Order Analysis	17
2.3.3	Second-Order Analysis	18
3	Erosion in a Channel	20
3.1	Governing Equations	20
3.2	Scaling and Non-Dimensionalization	20
3.3	Asymptotic Analysis	21
4	Elasticity of the Channel	22
4.1	Governing Equations	22
4.2	Scaling and Non-Dimensionalization	24
4.3	Asymptotic Analysis	25
4.3.1	Leading-Order Analysis	25
4.3.2	First-Order Analysis	27
5	Particle Concentration in the Channel	28

5.1	Governing Equations	28
5.2	Scaling and Non-dimensionalization	29
5.3	Asymptotic Analysis	29
5.3.1	Leading Order Analysis	30
5.3.2	First-Order Analysis	30
5.3.3	Second-Order Analysis	31
5.4	Final solution	32
6	Results	33
6.1	Channel with active erosion:	33
7	Conclusions	35
7.1	Conclusions/Extensions	35
8	Acknowledgements	36

Chapter 1

Introduction

Erosion and deposition of particles alter the solid interface and the internal morphology, then as a consequence affect properties of the flow, notably the fluid velocity, the exerted shear stress by the flow and the particle concentration in the feed. These two processes are ubiquitous within the nature as well as the industry, therefore investigating them is instrumental to address their desirability within fluid flow systems. Specific easily observable examples from geomorphology include soil erosion and land degradation (due to wind or floodwaters), erosion of riverbanks [19],[10] and formation of yardangs or pillar and toadstool-shaped rock formations known as hoodoos due to wind erosion [23]. Less obvious examples found in biology include the formation of arterial plaques, bacterial colonies known as biofilms, as well as the erosion and particle deposition in the porous media and membrane filters. In the environmental context, erosion represents the destruction of the mass caused by forces exerted on the contact interface between a solid and fluid phase over a long period. For instance, tunnel erosion is one type of erosion caused by water penetrating through a hole in a sub-surface; parts of the soil are carried away with flow and leaves behind a small tunnel underneath the surface. The tunnel becomes larger due to water flow resulting in a substantial likelihood for the soil to collapse. Generally speaking, in geological contexts, erosion of solid bodies and deposition of debris on or into them is essential in carving and shaping various morphologies in nature and the environment. The interactions of air and water with the Earth's surface

have been modeled and studied up to date; for example [16], [15], [14] and references. Similarly, fluid flow through a porous medium can erode and/or deposit particles and thereby change the morphology of the porous media, which results in altering the flow path [12]. Depending on the flow and the structure of the porous media, two scenarios will be considered in modeling of erosion and deposition: (i) external and (ii) internal flow within the geological structures and porous media. In the former case, it is assumed that the structure is porosity-graded and consists of a collection of solid obstacles or fibers, which fluid flow moves around them.

On the other hand for the internal flow, which is our focus, the structure is assumed to consist of slender channels/pores that span the structure from upstream to downstream side and the viscous fluid flow moves inside the channels/pores Fig. 1.1. For example, one may consider internal erosion in structures such as embankment dams [6] and porous media, which can be interpreted as reverse filtration and deposition processes [9]. There are, therefore, many mathematical similarities in the modeling of deposition and erosion processes. The purpose of our modeling effort is to propose a model tracing the deposition/erosion occurrence and their influences on the structure, given specific identifiable parameters. Different numerical schemes exist in the literature to model the erosion process. One of the approaches is the resolved computational Fluid Dynamics (CFD) method. Considerable effort has been devoted to solving this direct method. The fluid flow and particle interactions are investigated through basic empirical systems of formulas, where the governing equations are being solved using Finite Elements Methods (FEM), i.e. the Navier-Stokes equations are simulated using a collocated mesh grid in which the pore geometry defines the structure. Each step taken towards convergence is expensive and adaptive re-meshing is often used to account for micro-structure evolution. Therefore, many other authors considered a second approach using an unresolved CFD approach consisting of a coupled hybrid model. Numerous works adopted this newly emerged technique to investigate further the fluid path after a reconfiguration of the system structure. This technique is less expensive to implement solving the considered equations on fluid cells much larger than the pore scale level. It does not require re-meshing,

and thus, the microscopic description of the problem is comparatively inefficient. The third approach is the Lattice-Boltzmann Methods (LBM), which consists for discretizing the particle-based model and solving for the flow on a pore-scale level, replacing the Navier Stokes equations by the discrete Boltzmann equation. The fluid/particle behavior is resolved through interpolation and extrapolation schemes, modeling the Navier Stokes equation beyond the known points by drawing a likely approximate form through a fixed lattice. Similarly to the CFD, this technique stimulates the fluid behavior by discretizing the flow velocity vectors relative to the pore scale. Despite its high ability to resolve a three-dimensional lattice, LBM is an expensive method to implement and requires high computation power. The fourth approach is the pore network model (PNM), which consists of simplifying the system geometry into pore spaces interconnected via their respective inlet structure. The complexity of the flow is, therefore, reduced to the exchange laws between the adjacent edges. The formulation of the flow equation is based on the assumption of a unique pressure at each computational node. This technique achieves high-resolution accuracy running on small scale domains using lower computing costs, compared to other simulation methods such LBM.

Looking at the Membrane filters, they are used in many industrial engineering processes that require separating particles and contaminants of any given size from a fluid. Water purification [11], many separation processes in the biotech industry [1], treatment of radioactive sludge, and beer clarification are just a few of the widespread applications. The details of the filtration in these applications may vary dramatically depending on the size of particles to be removed, the flow speed of the particle-laden solvent, the rigidity of the particles and so on; however, maintaining the desired separation control at a reasonable flow rate, using the least energy possible, is usually the ultimate goal. Therefore, for a given application, membrane filters with specific characteristics such as flat or pleated [20], specific internal structure, specific pore sizes and shape [17], pore connectivity and distribution within the membrane [8] may be needed. A multilayered membrane consists of a stack of membranes, with different physical properties such as pore size and porosity, usually laminated at the layer junctions. Multilayered membranes

are used widely in a variety of industrial applications, such as separation of cells or particles [8], or they can be combined to form the filtration support layers required in ultrafiltration, gas separation, and catalysis [13]. It has been demonstrated experimentally that a well-designed multilayer membrane performs better (according to a range of selected performance criteria) than a homogeneous membrane [24]. Mathematical characterization and modeling of multilayered membranes can help our understanding of how the properties of each layer affect the performance of the overall membrane stack. Various models that attempt to analyze the performance of multilayered membrane filters have been formulated and examined to date. For instance, simple network models, in which the porous material is represented by a rectangular network where bonds and nodes represent pores and inter-pore connections (with each pore represented by a straight cylindrical capillary of specified length and diameter), respectively, have been studied by several authors. Such network models can quickly generate performance data, such as flux and particle retention characteristics, for a broad sweep of filter geometries (membrane microstructures). Early variants of such models [5] assume identical pores, but more recent versions [17] attempt to capture the depth variation of pore structure that is engineered in real membranes, allowing pore size and connectivity to be a function of depth through the membrane by adopting a layered structure, with changes in pore size/connectivity occurring at layer boundaries. An important application of such models is in identifying optimal configurations for the pore microstructure, in terms of (for example) maximizing throughput of filtered fluid and filter lifetime, while removing an acceptable fraction of particles. Particles removed by the filter inevitably foul it, via three principal distinct fouling modes: (a) standard blocking or adsorptive fouling, in which particles smaller than the membrane pores are deposited or adsorbed within pores and shrink the pore radius; (b) blocking (complete or partial) of pores by large particles, which are “sieved” from the fluid; and (c) cake formation (once pores are blocked by large particles, other particles can accumulate on top of the membrane, forming a “cake” layer, adding additional resistance via a secondary porous layer on top) [1],[18],[4], [7] Many studies, both experimental and theoretical, have shown that a negative porosity gradient in the depth

of the filter can improve filter efficiency as measured by, for example, the total volume of filtrate fluid processed by the filter over its lifetime; the energy consumed in obtaining the filtrate; and also the level of contaminant remaining in the filtrate. This may be understood by noting that filter fouling necessarily is heaviest at the upstream side of the filter, where the feed suspension enters, thus this side needs to be more porous than the downstream side in order to deal with the heavier fouling burden. Filtration efficiency considerations are complicated by the frequent need for a very clean filtrate, which inevitably means that a large (downstream) portion of the filter membrane must remain nearly unfouled [8]. On the other hand, Cell proliferation within a fluid-filled porous tissue-engineering scaffold depends on a sensitive choice of pore geometry and flow rates: regions of high curvature encourage cell proliferation, while a critical flow rate is required to promote growth for certain cell types. When the flow rate is too slow, the nutrient supply is limited; when it is too fast, cells may be damaged by the high fluid shear stress. As a result, determining appropriate tissue-engineering-construct geometries and operating regimes poses a significant challenge that cannot be addressed by experimentation alone.

In this report, we present a mathematical theory for the fluid flow within a pore of a tissue-engineering scaffold, which is coupled to the growth of cells on the pore walls. We exploit the slenderness of a pore that is typical in such a scenario, to derive a reduced model that enables a comprehensive analysis of the system to be performed. We derive analytical solutions in a particular case of a nearly piecewise constant growth law and compare these with numerical solutions of the reduced model. Qualitative comparisons of tissue morphologies predicted by our model, with those observed experimentally, are also made.

Also, we take an integrated approach to formulate and study mathematical models of deposition and erosion in re-configurable flow networks, in geologic structures and other materials, alongside analytically exact validation from experimental data. The experiments will help calibrate and validate the mathematical models, and of course are much cheaper than gathering data from real-world examples. The paper is organized as follows:

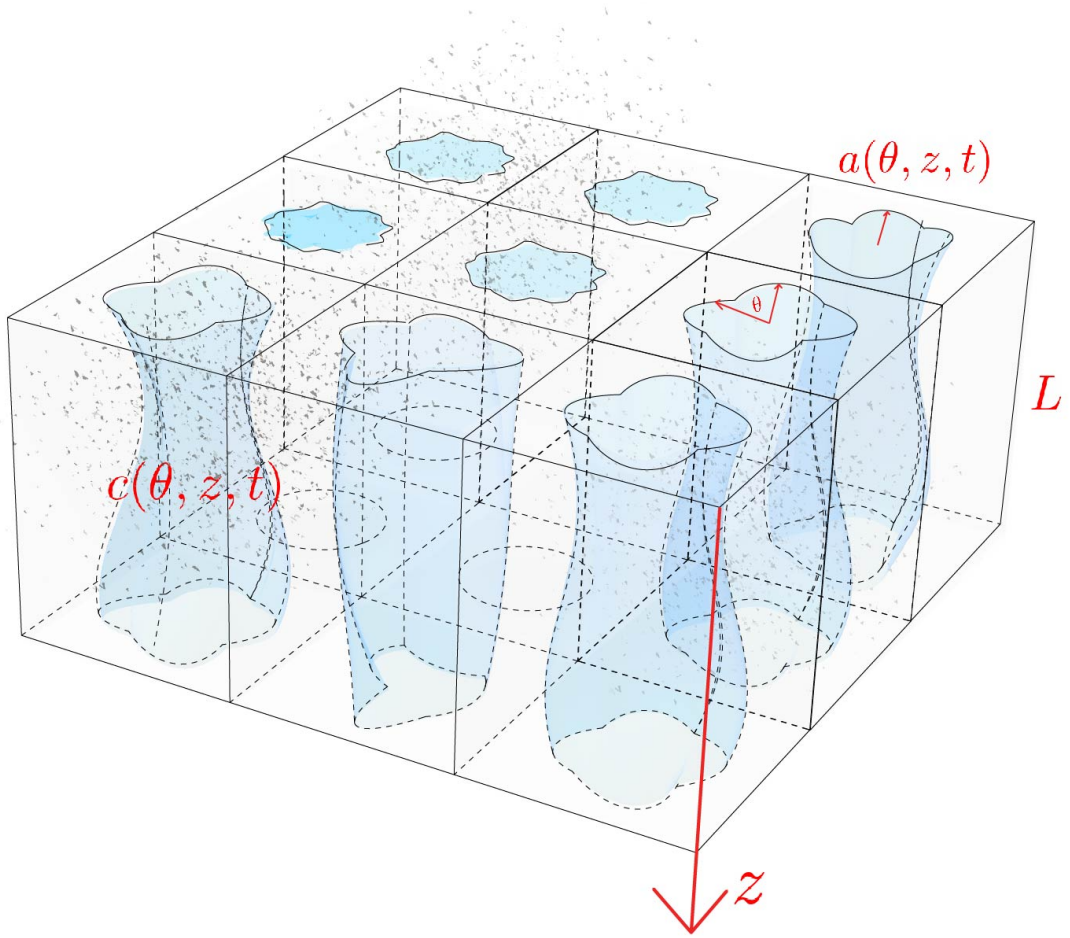


Figure 1.1: Schematic showing a structure and channels with the pore radii $a(\theta, z, t)$ and small-particle concentration $c(\theta, z, t)$.

(a) we introduce the mathematical model for flow in a channel, as well as the governing equations of particles in the fees. (b) We introduce appropriate scaling, for the flow and particles concentration, to non-dimensionalize the models from ‘a’. Then, (c) We present simulations that address the erosion and deposition of particles in a structure, specifically the pore evolution under the erosion and deposition scenarios. Finally, we summarize our modeling results and provide some insight into real-world applications as well [3].

Chapter 2

Flow in a Channel

Let's started by introducing the dimensional and dimensionless parameters:

Parameter	Description
Q_i	Inlet flux
R	Fluid-cell-layer interface radius
L	Fluid-cell-layer interface length
ϵ	Dimensionless fluid-cell-layer interface aspect ratio
μ	Fluid viscosity
p	Pressure drop across membrane
c	Total concentration of particles in feed suspension
ζ	Dimensionless pressure drop across the length of the pore

2.1 Governing Equations

In order to model the fluid flow, we consider a low Reynolds number, which leads to the inertia term within the Navier-Stokes equation to be neglected. This results in the pore velocity $\mathbf{u} = (u, v, w)$ satisfying the Stokes equation

$$\nabla p = \mu \nabla^2 \mathbf{u}, \quad \nabla \cdot \mathbf{u} = 0, \quad (2.1)$$

where p represents the pressure along the channel, μ is the viscosity of the fluid. These equation must satisfy the following boundary conditions:

$$u = v = w = 0 \quad \text{at} \quad r = a(\theta, z, t). \quad (2.2)$$

We also enforce the no-slip and no penetration boundary conditions along with the symmetry condition

$$u = v = \frac{\partial w}{\partial r} = 0 \quad \text{at} \quad r = 0. \quad (2.3)$$

We consider a constant flux scenario along the channel, where we define the pressure at the inlet as $p = \zeta(t)$ at $z = 0$, and a trivial pressure $p = 0$ at $z = L$, the outlet of the channel. Therefore, enforcing constant fluid flux we obtain,

$$\int_0^{2\pi} \int_0^a |\mathbf{u}| r dr d\theta = Q_i, \quad (2.4)$$

where Q_i is the inlet flux of flow at the top of the channel. In order to close our model, we consider the shear forces exerted by the fluid flow at the wall of the channel given by

$$\sigma_s = \mu (\nabla \mathbf{u} + \nabla \mathbf{u}^T) \mathbf{n} \cdot \mathbf{t} \Big|_{r=a(\theta, z, t)} \quad (2.5)$$

$$= \sqrt{\boldsymbol{\tau} \cdot \boldsymbol{\tau} - |\boldsymbol{\tau} \cdot \mathbf{n}|^2}. \quad (2.6)$$

\mathbf{n} is the unit normal to the wall and is defined as $n = \frac{\nabla(r-a)}{|\nabla(r-a)|}$ and \mathbf{t} is the unit tangential vector to the channel wall. Writing equation (2.1) in cylindrical coordinates yields:

$$\frac{\partial p}{\partial r} = \mu \left[\frac{1}{r} \frac{\partial}{\partial r} \left(r \frac{\partial u}{\partial r} \right) + \frac{1}{r^2} \frac{\partial^2 u}{\partial \theta^2} + \frac{\partial^2 u}{\partial z^2} - \frac{u}{r^2} - \frac{2}{r^2} \frac{\partial v}{\partial \theta} \right], \quad (2.7)$$

$$\frac{1}{r} \frac{\partial p}{\partial \theta} = \mu \left[\frac{1}{r} \frac{\partial}{\partial r} \left(r \frac{\partial v}{\partial r} \right) + \frac{1}{r^2} \frac{\partial^2 v}{\partial \theta^2} + \frac{\partial^2 v}{\partial z^2} - \frac{v}{r^2} + \frac{2}{r^2} \frac{\partial u}{\partial \theta} \right], \quad (2.8)$$

$$\frac{\partial p}{\partial z} = \mu \left[\frac{1}{r} \frac{\partial}{\partial r} \left(r \frac{\partial w}{\partial r} \right) + \frac{1}{r^2} \frac{\partial^2 w}{\partial \theta^2} + \frac{\partial^2 w}{\partial z^2} \right], \quad (2.9)$$

$$\frac{1}{r} \frac{\partial}{\partial r} (ru) + \frac{1}{r} \frac{\partial v}{\partial \theta} + \frac{\partial w}{\partial z} = 0. \quad (2.10)$$

These equations must be solved subject to the following boundary conditions representing enforcing no slip and no penetration at the fluid-cell-layer interface, as well as the symmetry conditions respectively:

$$u = v = w = 0 \quad \text{at} \quad r = a(\theta, z, t), \quad \text{and} \quad u = v = \frac{\partial w}{\partial r} \quad \text{at} \quad r = 0. \quad (2.11)$$

Similarly, we expand the velocity variable componentwisely to obtain:

$$\int_0^{2\pi} \int_0^a \sqrt{u^2 + v^2 + w^2} r dr d\theta = Q_i. \quad (2.12)$$

Next, we expand the shear stress from (2.6) as

$$\boldsymbol{\tau} = \mu \begin{bmatrix} 2 \frac{\partial u}{\partial r} & \frac{1}{r} \frac{\partial u}{\partial \theta} - \frac{v}{r} + \frac{\partial v}{\partial r} & \frac{\partial u}{\partial z} + \frac{\partial w}{\partial r} \\ \frac{1}{r} \frac{\partial u}{\partial \theta} - \frac{v}{r} + \frac{\partial v}{\partial r} & 2 \left(\frac{1}{r} \frac{\partial v}{\partial \theta} + \frac{u}{r} \right) & \frac{\partial v}{\partial z} + \frac{1}{r} \frac{\partial v}{\partial \theta} \\ \frac{\partial u}{\partial z} + \frac{\partial w}{\partial r} & \frac{\partial v}{\partial z} + \frac{1}{r} \frac{\partial v}{\partial \theta} & 2 \frac{\partial w}{\partial z} \end{bmatrix} \cdot \mathbf{n}, \quad (2.13)$$

where we derive the normal vector to the channel wall as follows:

$$\begin{aligned} \mathbf{n} &= \frac{\nabla(r-a)}{|\nabla(r-a)|} \\ &= \frac{1}{\sqrt{\left| \frac{\partial(r-a)}{\partial r} \right|^2 + \left| \frac{1}{r} \frac{\partial(r-a)}{\partial \theta} \right|^2 + \left| \frac{\partial(r-a)}{\partial z} \right|^2}} \left(\frac{\partial(r-a)}{\partial r}, \frac{1}{r} \frac{\partial(r-a)}{\partial \theta}, \frac{\partial(r-a)}{\partial z} \right) \\ &= \frac{1}{\sqrt{1 + \frac{1}{r^2} a_\theta^2 + a_z^2}} \left(1, -\frac{1}{r} a_\theta, a_z \right). \end{aligned} \quad (2.14)$$

2.2 Scaling and Non-Dimensionalization

We introduce the following scalings, where given arbitrary variable x , \hat{x} denotes x in dimensionless form [17]:

$$\begin{aligned}
\frac{R}{L} &= \epsilon \ll 1, \\
\mathbf{u} &= \frac{Q_i}{\pi R^2} \mathbf{u} = \frac{Q_i}{\pi R^2} (\epsilon \hat{u}, \epsilon \hat{v}, \hat{w}), \\
(p, \zeta) &= \frac{\mu L Q_i}{\pi R^4} (\hat{p}, \hat{\zeta}), \\
(r, a, z) &= L (\epsilon \hat{r}, \epsilon \hat{a}, \hat{z}), \\
(\boldsymbol{\tau}, \sigma_s) &= \frac{\mu Q_i}{\pi R^3} (\hat{T}, \hat{\sigma}_s).
\end{aligned} \tag{2.15}$$

Using the scaling, we can express the governing flow equations as follows. For simplicity, we drop hats.

$$\frac{1}{\epsilon^2} \frac{\partial p}{\partial r} = \frac{1}{r} \frac{\partial}{\partial r} \left(r \frac{\partial u}{\partial r} \right) + \frac{1}{r^2} \frac{\partial^2 u}{\partial \theta^2} + \epsilon^2 \frac{\partial^2 u}{\partial z^2} - \frac{u}{r^2} - \frac{2}{r^2} \frac{\partial v}{\partial \theta}, \tag{2.16}$$

$$\frac{1}{\epsilon^2} \frac{1}{r} \frac{\partial p}{\partial \theta} = \frac{1}{r} \frac{\partial}{\partial r} \left(r \frac{\partial v}{\partial r} \right) + \frac{1}{r^2} \frac{\partial^2 v}{\partial \theta^2} + \epsilon^2 \frac{\partial^2 v}{\partial z^2} - \frac{v}{r^2} + \frac{2}{r^2} \frac{\partial u}{\partial \theta}, \tag{2.17}$$

$$\frac{\partial p}{\partial z} = \frac{1}{r} \frac{\partial}{\partial r} \left(r \frac{\partial w}{\partial r} \right) + \frac{1}{r^2} \frac{\partial^2 w}{\partial \theta^2} + \epsilon^2 \frac{\partial^2 w}{\partial z^2}, \tag{2.18}$$

$$\frac{1}{r} \frac{\partial}{\partial r} (ru) + \frac{1}{r} \frac{\partial v}{\partial \theta} + \frac{\partial w}{\partial z} = 0. \tag{2.19}$$

The boundary condition and velocity variables become

$$u = v = w = 0 \quad \text{at} \quad r = a(\theta, z, t), \quad \text{and} \quad u = v = \frac{\partial w}{\partial r} \quad \text{at} \quad r = 0, \tag{2.20}$$

$$p = \zeta(t) \quad \text{at} \quad z = 0, \quad \text{and} \quad p = 0 \quad \text{at} \quad z = 1, \tag{2.21}$$

$$\int_0^{2\pi} \int_0^a \sqrt{\epsilon^2 u^2 + \epsilon^2 v^2 + w^2} r \, dr d\theta = \pi. \tag{2.22}$$

Therefore, the shear stress in (2.13) now become

$$\boldsymbol{\tau} = \mu \begin{bmatrix} 2\epsilon \frac{\partial u}{\partial r} & \epsilon \left(\frac{1}{v} \frac{\partial u}{\partial \theta} - \frac{v}{r} + \frac{\partial v}{\partial r} \right) & \epsilon^2 \frac{\partial u}{\partial z} + \frac{\partial u}{\partial r} \\ \epsilon \left(\frac{1}{v} \frac{\partial u}{\partial \theta} - \frac{v}{r} + \frac{\partial v}{\partial r} \right) & 2\epsilon \left(\frac{1}{r} \frac{\partial v}{\partial \theta} + \frac{u}{r} \right) & \epsilon^2 \frac{\partial v}{\partial z} + \frac{1}{r} \frac{\partial u}{\partial \theta} \\ \epsilon^2 \frac{\partial u}{\partial z} + \frac{\partial u}{\partial r} & \epsilon^2 \frac{\partial v}{\partial z} + \frac{1}{r} \frac{\partial u}{\partial \theta} & 2\epsilon \frac{\partial w}{\partial z} \end{bmatrix} \cdot \mathbf{n}, \quad (2.23)$$

where the normal vector to the wall is:

$$\mathbf{n} = \frac{1}{\sqrt{1 + \frac{1}{r^2} \left(\frac{\partial a}{\partial \theta} \right)^2 + \epsilon^2 \left(\frac{\partial a}{\partial z} \right)^2}} \left(1, -\frac{1}{r} \frac{\partial a}{\partial \theta}, -\epsilon \frac{\partial a}{\partial z} \right).$$

2.3 Asymptotic Analysis

The complete system described in the above section is extremely hard to solve analytically, and is also computationally costly to solve numerically in a brute force way. We make use of the fact that the pore aspect ratio $\epsilon = R/L \ll 1$. This allows us to achieve a simpler, computationally-feasible, reduced asymptotic model. We also assume that the channel radius is roughly circular with small axial and azimuthal variation, we determine the dependence of the change of channel radius on the axial and azimuthal coordinates at first order in the pore aspect ratio ϵ . We assume that the channel radius is expressed as

$$a(\theta, z, t) = a_0(t) + \epsilon a_1(\theta, z, t), \quad (2.24)$$

where

$$a_1(\theta, z, t) = \Lambda(z, t) \cos(n\theta) + \Upsilon(z, t), \quad (2.25)$$

where $\Lambda(z, t)$ and $\Upsilon(z, t)$ are functions to be pinned down and n is an integer that describes the number of lobes in the geometry of the underlying substrate. Although the above assumption imposes constraints on the class of channels we can study, this assumption is later to be found essential in attaining a balance between some level of generality and feasible asymptotic calculations. Here the initial configuration of the channel radius $a(\theta, z, 0)$ is given by the shape of the underlying substrate, and its subsequent evolution

is described by the equation of erosion, elasticity and deposition equations, which will be explained in next chapters. Below, we asymptotically expand the variables u , v , w , p , ζ and σ_s in the form

$$x = x_0 + \epsilon x_1 + \mathcal{O}(\epsilon^2), \quad (2.26)$$

where x is any variable listed above.

2.3.1 Leading-Order Analysis

Rewriting (2.16) and (2.17) at $\mathcal{O}(1/\epsilon^2)$ gives

$$\frac{\partial p_0}{\partial r} = 0, \quad \frac{1}{r} \frac{\partial p_0}{\partial \theta} = 0, \quad (2.27)$$

At $\mathcal{O}(1)$, (2.18) gives

$$\frac{\partial p_0}{\partial z} = \frac{1}{r} \frac{\partial}{\partial r} \left(r \frac{\partial w_0}{\partial r} \right) + \frac{1}{r^2} \frac{\partial^2 w_0}{\partial \theta^2}. \quad (2.28)$$

For the channel wall configuration (2.25), the flow will be independent of θ , therefore (2.28) simplifies to

$$\frac{\partial p_0}{\partial z} = \frac{1}{r} \frac{\partial}{\partial r} \left(r \frac{\partial w_0}{\partial r} \right), \quad (2.29)$$

According to no slip boundary condition (2.11) where $w(a) = 0$, we have the equation

$$w_0(a_0 + \epsilon a_1 + \dots) + \epsilon w_1(a_0 + \epsilon a_1 + \dots) + \mathcal{O}(\epsilon^2) = 0.$$

By using Taylor expansions and matching coefficients, we have:

$$w_0 \Big|_{r=a_0} = 0, \quad \frac{\partial w_0}{\partial r} \Big|_{r=0} = 0. \quad (2.30)$$

Solve (2.28) with (2.30) together, we get:

$$w_0 = \frac{1}{4} \frac{dp_0}{dz} (r^2 - a_0^2) \quad (2.31)$$

Plug it into (2.22), simplify the results and match the coefficients of $\mathcal{O}(\epsilon)$, we get:

$$\mathcal{O}(1) : \quad \int_0^{2\pi} \int_0^{a_0} w_0 r dr d\theta = \pi \quad (2.32)$$

$$\mathcal{O}(\epsilon) : \quad \int_0^{2\pi} \int_0^{a_0} w_1 r dr d\theta = 0 \quad (2.33)$$

Solving the integrals, we obtain the following solutions:

$$u_0 = v_0 = 0 \quad (2.34)$$

$$w_0 = \frac{\zeta_0}{4} (a_0^2 - r^2) \quad (2.35)$$

$$\zeta_0 = \frac{8}{a_0^4} \quad (2.36)$$

$$p_0 = \zeta_0 (1 - z) \quad (2.37)$$

2.3.2 First-Order Analysis

At $\mathcal{O}(\epsilon)$, using similar technique, we seek a θ -independent solution to the governing equations, we find:

$$w_1 = \left[\frac{\Lambda}{2} a_0^{1-n} r^n \cos n\theta + \frac{\Upsilon}{2a_0} (2r^2 - a_0^2) \right] \zeta_0 \quad (2.38)$$

$$p_1 = \frac{4\zeta_0}{a_0} \int_1^z \Upsilon(z') dz' \quad (2.39)$$

$$\zeta_1 = -\frac{4\zeta_0}{a_0} \int_1^z \Upsilon(z') dz' \quad (2.40)$$

2.3.3 Second-Order Analysis

Similarly as previous analysis, plug (2.31) and (2.39) into (2.22), we obtain:

$$\int_0^{2\pi} \int_0^a \left[\frac{\Lambda}{2} a_0^{1-n} r^n \cos(n\theta) + \frac{1}{4\zeta_0} \frac{dP_1}{dz} (r^2 - a_0^2) + a_0 \frac{\Upsilon(z)}{2} \right] r \, dr d\theta = 0. \quad (2.41)$$

We expand the shear stress as:

$$\boldsymbol{\tau} = \begin{bmatrix} \mathcal{O}(\epsilon^2) & \mathcal{O}(\epsilon^2) & \frac{\partial w_0}{\partial r} + \epsilon \frac{\partial w_1}{\partial r} + \mathcal{O}(\epsilon^2) \\ \mathcal{O}(\epsilon^2) & \mathcal{O}(\epsilon^2) & \frac{\epsilon}{r} \frac{\partial w_1}{\partial \theta} + \mathcal{O}(\epsilon^2) \\ \frac{\partial w_0}{\partial r} + \epsilon \frac{\partial w_1}{\partial r} + \mathcal{O}(\epsilon^2) & \frac{\epsilon}{r} \frac{\partial w_1}{\partial \theta} + \mathcal{O}(\epsilon^2) & 2\epsilon \frac{\partial w_0}{\partial r} + \mathcal{O}(\epsilon^2) \end{bmatrix} \begin{bmatrix} 1 \\ \mathcal{O}(\epsilon) \\ \mathcal{O}(\epsilon^2) \end{bmatrix},$$

$$\boldsymbol{\tau}|_{r=a_0} = \begin{bmatrix} \mathcal{O}(\epsilon^2) \\ \mathcal{O}(\epsilon^2) \\ \frac{\partial w_0}{\partial r} + \epsilon \frac{\partial w_1}{\partial r} + \mathcal{O}(\epsilon^2) \end{bmatrix},$$

$$\boldsymbol{\tau} \cdot \mathbf{n} = \mathcal{O}(\epsilon^2), \quad (2.42)$$

where we derive the normal vector to the wall as follows:

$$\mathbf{n} = \left(1, -\frac{\epsilon}{r} \frac{\partial a_1}{\partial \theta}, -\epsilon^2 \frac{\partial a_1}{\partial z} \right). \quad (2.43)$$

$$\begin{aligned} \sigma_s &= \sqrt{\boldsymbol{\tau} \cdot \boldsymbol{\tau} - |\boldsymbol{\tau} \cdot \mathbf{n}|^2}|_{r=a_0} \\ &= \left| \left[\frac{\partial w_0}{\partial r} + \epsilon \frac{\partial w_1}{\partial r} \right] \Big|_{r=a_0} \right| \\ &= -\frac{\zeta_0 a_0}{2} + \epsilon \left(\frac{n\Lambda}{2} \cos(n\theta) + 2\Upsilon \right) \zeta_0 \end{aligned} \quad (2.44)$$

Set

$$\sigma_s = \sigma_{s_0}(t) + \epsilon \left(\sigma_{s_{1,a}}(z, t) \cos(n\theta) + \sigma_{s_{1,b}}(z, t) \right) \quad (2.45)$$

Matching the coefficients of (2.44) and (2.45), we get:

$$\begin{aligned}\sigma_{s_0}(t) &= \frac{\zeta_0(t)a_0}{2} \\ \sigma_{s_{1,a}}(z, t) &= \frac{n\Lambda\zeta_0}{2} \\ \sigma_{s_{1,b}}(z, t) &= 2\Upsilon\zeta_0\end{aligned}\tag{2.46}$$

Chapter 3

Erosion in a Channel

3.1 Governing Equations

The fluid exerts forces on the wall of the channel and subsequently its radius responds by expansion as follows:

$$\frac{\partial a}{\partial t} = \lambda f(\sigma_s), \quad (3.1)$$

3.2 Scaling and Non-Dimensionalization

We use the scalings from (2.15) along with the time scaling

$$t = \frac{\pi R^4}{\lambda \mu Q_i} \hat{t}, \quad (3.2)$$

After dropping hats, (3.1) and (3.2) gives

$$\frac{\partial a}{\partial t} = f(\sigma_s). \quad (3.3)$$

3.3 Asymptotic Analysis

Using (2.25) and (3.2), we can obtain:

$$\frac{\partial a_0}{\partial t} + \epsilon \left(\frac{\partial \Lambda}{\partial t} \cos(n\theta) + \frac{\partial \Upsilon}{\partial t} \right) = \lambda \sigma_{s_0}(t) + \epsilon \left(\sigma_{s_{1,a}}(z, t) \cos(n\theta) + \sigma_{s_{1,b}}(z, t) \right) \quad (3.4)$$

Matching the corresponding terms using (2.46), we get:

$$\frac{\partial a_0}{\partial t} = \frac{4\lambda}{a_0^3} \quad (3.5)$$

$$\frac{\partial \Lambda(t)}{\partial t} = \frac{4n\lambda}{a_0^4} \Lambda(t) \quad (3.6)$$

$$\frac{\partial \Upsilon}{\partial t} = \frac{16\lambda}{a_0^4} \Upsilon(t) \quad (3.7)$$

Solving the three equations above, we obtain

$$a_0(t) = (16\lambda t + a_0^4(0))^{\frac{1}{4}} \quad (3.8)$$

$$\Lambda(t) = \Lambda(0) \left[\frac{16\lambda t + a_0^4(0)}{a_0^4(0)} \right]^{\frac{n}{4}} \quad (3.9)$$

$$\Upsilon(t) = \Upsilon(0) \left[\frac{16\lambda t + a_0^4(0)}{a_0^4(0)} \right] \quad (3.10)$$

Chapter 4

Elasticity of the Channel

4.1 Governing Equations

We now want to consider elasticity of the material of the wall of the channels. Let $\Omega = (\Omega_x, \Omega_y, \Omega_z)$ be the displacement of the channel. The displacement is modeled by the Navier-Cauchy equation

$$\frac{E}{2(1+\nu)}\nabla^2\Omega + \frac{E}{2(1+\nu)(1-2\nu)}\nabla(\nabla\cdot\Omega) = \rho_m\left(\frac{\partial^2\Omega}{\partial T^2}\right), \quad (4.1)$$

where E is Young's modulus, ν is Poisson's ratio, and T is time [22]. We assume that the time scale of the fluid dynamics in the problem is much smaller than the elastic response of the channel material to the hydraulic stress. Therefore, the right hand side of (4.1) is negligibly small. Once we simplify Eq. (4.1), we get

$$\nabla^2\Omega + \frac{E}{2(1-\nu)(1-2\nu)}\nabla(\nabla\cdot\Omega) = 0. \quad (4.2)$$

In our set up the channels are clamped above and below. Therefore,

$$\Omega \Big|_{z=0} = \Omega \Big|_{z=L} = 0 \quad (4.3)$$

We have that the strain in the radial direction at the boundary is the pressure p .

$$\sigma_r \Big|_{r=a} = p \quad (4.4)$$

We also assume that the the strain is symmetric across channels which suggests that

$$\frac{\partial \sigma_r}{\partial r} \Big|_{r=R} = 0 \quad (4.5)$$

Given the near-cylindrical shape of our channels, it is natural to work on cylindrical coordinates. Transforming (4.2) under cylindrical coordinates we get

$$\Omega = (\Omega_r, \Omega_\theta, \Omega_z) \quad (4.6)$$

$$\nabla^2 \Omega_r - \frac{\Omega_r}{r^2} - \frac{2}{r^2} \frac{\partial \Omega_\theta}{\partial \theta} + \frac{1}{1-2\nu} \frac{\partial}{\partial r} (\nabla \cdot \Omega) = 0 \quad (4.7)$$

$$\nabla^2 \Omega_\theta - \frac{\Omega_\theta}{r^2} - \frac{2}{r^2} \frac{\partial \Omega_r}{\partial \theta} + \frac{1}{r} \frac{1}{1-2\nu} \frac{\partial}{\partial \theta} (\nabla \cdot \Omega) = 0 \quad (4.8)$$

$$\nabla^2 \Omega_z + \frac{1}{1-2\nu} \frac{\partial}{\partial z} (\nabla \cdot \Omega) = 0 \quad (4.9)$$

where $\nabla = (\frac{\partial}{\partial r}, \frac{1}{r} \frac{\partial}{\partial \theta}, \frac{\partial}{\partial z})$

We also have the strain-displacement equations which model the interaction of the strain and displacement of the channel wall [22].

$$\sigma_r = \frac{E(1-\nu)}{(1+\nu)(1-2\nu)} \frac{\partial \Omega_r}{\partial r} + \frac{E\nu}{(1+\nu)(1-2\nu)} \frac{1}{2} \left(\frac{\partial \Omega_\theta}{\partial \theta} + \Omega_r \right) \quad (4.10)$$

$$\sigma_\theta = \frac{E\nu}{(1+\nu)(1-2\nu)} \frac{\partial \Omega_r}{\partial r} + \frac{E(1-\nu)}{(1+\nu)(1-2\nu)} \frac{1}{2} \left(\frac{\partial \Omega_\theta}{\partial \theta} + \Omega_r \right) \quad (4.11)$$

$$\sigma_z = \frac{E\nu}{(1+\nu)(1-2\nu)} \frac{\partial \Omega_r}{\partial r} + \frac{E\nu}{(1+\nu)(1-2\nu)} \frac{1}{r} \left(\frac{\partial \Omega_\theta}{\partial \theta} + \Omega_r \right) + \frac{E(1-\nu)}{(1+\nu)(1-2\nu)} \frac{\partial \Omega_z}{\partial z} \quad (4.12)$$

4.2 Scaling and Non-Dimensionalization

As before we want to scale parameters in order to work with dimensionless parameters.

We use the following scaling.

$$\begin{aligned} (r, a, z) &= L(\epsilon \hat{r}, \epsilon \hat{a}, \hat{z}) \\ (\Omega_r, \Omega_\theta, \Omega_z) &= R(\hat{\Omega}_r, \epsilon \hat{\Omega}_\theta, \hat{\Omega}_z) \\ (\sigma, p) &= \frac{\mu L Q_i}{\pi R^4} (\hat{\sigma}, \hat{p}) \end{aligned}$$

for some small $\epsilon = R/L \ll 1$ [2]. Here we have added hats to indicate new variables but shall drop them from now on. Under this scaling and cylindrical coordinates, (4.7), (4.8), and (4.9), become

$$\begin{aligned} \frac{1}{r} \frac{\partial}{\partial r} \left(r \frac{\partial \Omega_r}{\partial r} \right) + \frac{1}{r^2} \frac{\partial^2 \Omega_r}{\partial \theta^2} + \epsilon^2 \frac{\partial^2 \Omega_r}{\partial z^2} - \frac{\Omega_r}{r^2} - \frac{2}{r^2} \epsilon \frac{\partial \Omega_\theta}{\partial \theta} \\ + \frac{1}{1-2\nu} \frac{\partial}{\partial \theta} \left[\frac{1}{r} \frac{\partial}{\partial r} (r \Omega_r) + \epsilon \frac{1}{r} \frac{\partial \Omega_\theta}{\partial \theta} + \epsilon \frac{\partial \Omega_z}{\partial z} \right] = 0, \end{aligned} \quad (4.13)$$

$$\begin{aligned} \frac{\epsilon}{r} \frac{\partial}{\partial r} \left(r \frac{\partial \Omega_\theta}{\partial r} \right) + \frac{\epsilon}{r^2} \frac{\partial^2 \Omega_\theta}{\partial \theta^2} + \epsilon^2 \frac{\partial^2 \Omega_\theta}{\partial z^2} - \epsilon \frac{\Omega_\theta}{r^2} - \frac{2}{r^2} + \frac{2}{r^2} \frac{\partial \Omega_r}{\partial \theta} \\ + \frac{1}{1-2\nu} \frac{1}{r} \frac{\partial}{\partial \theta} \left[\frac{1}{r} \frac{\partial}{\partial r} (r \Omega_r) + \epsilon \frac{1}{r} \frac{\partial \Omega_\theta}{\partial \theta} + \epsilon \frac{\partial \Omega_z}{\partial z} \right] = 0, \end{aligned} \quad (4.14)$$

and

$$\begin{aligned} \frac{1}{r} \frac{\partial}{\partial r} \left(r \frac{\partial \Omega_z}{\partial r} \right) + \frac{1}{r^2} \frac{\partial^2 \Omega_z}{\partial \theta^2} + \epsilon^2 \frac{\partial^2 \Omega_z}{\partial z^2} \\ + \frac{1}{1-2\nu} \epsilon \frac{\partial}{\partial z} \left[\frac{1}{r} \frac{\partial}{\partial r} (r \Omega_r) + \epsilon^2 \frac{1}{r} \frac{\partial \Omega_\theta}{\partial \theta} + \epsilon \frac{\partial \Omega_z}{\partial z} \right] = 0 \end{aligned} \quad (4.15)$$

After scaling and rewriting the strain-displacement equations (4.10), (4.11), (4.12) and dropping the hat notation respectively, we have

$$\sigma_r = \frac{\pi ER^5}{(1+v)(1-2v)L\mu Q_i} \left[(1-v) \frac{\partial \Omega_r}{\partial r} + v \frac{1}{r} \left(\frac{\partial \Omega_\theta}{\partial \theta} + \Omega_r \right) + v\epsilon \frac{\partial \Omega_z}{\partial z} \right] \quad (4.16)$$

$$\sigma_\theta = \frac{\pi ER^4}{(1+v)(1-2v)L\mu Q_i} \left[v \frac{\partial \Omega_r}{\partial r} + (1-v) \frac{1}{r} \left(\frac{\partial \Omega_\theta}{\partial \theta} + \Omega_r \right) + v\epsilon \frac{\partial \Omega_z}{\partial z} \right] \quad (4.17)$$

$$\sigma_z = \frac{\pi ER^4}{(1+v)(1-2v)L\mu Q_i} \left[v \frac{\partial \Omega_r}{\partial r} + v \frac{1}{r} \left(\frac{\partial \Omega_\theta}{\partial \theta} + \Omega_r \right) + (1-v)\epsilon \frac{\partial \Omega_z}{\partial z} \right] \quad (4.18)$$

For sake of simplicity, let $\frac{1}{\eta} = \frac{\pi ER^5}{(1+v)(1-2v)L\mu Q_i}$.

Lastly, we scale our boundary conditions (4.3) - (4.5) and we get

$$\sigma_r \Big|_{r=a} = p \quad \frac{\partial \sigma_r}{\partial r} \Big|_{r=1} = 0 \quad \Omega_z \Big|_{z=0} = \Omega_z \Big|_{z=L} = 0 \quad (4.19)$$

We assume $\frac{\partial}{\partial \theta} \Omega = 0$ and $\Omega_\theta = 0$. Since the channel is nearly cylindrical we expect most displacement would be radially and vertically. Using these dimensionless equations, in the next sections we are going to perform an asymptomatic analysis of the system of equations.

4.3 Asymptotic Analysis

4.3.1 Leading-Order Analysis

Next, we are going to introduce an extension of our variables Ω, p with powers of $\epsilon \ll 1$.

Thus we get that:

$$\Omega_r = \Omega_{r,0} + \epsilon \Omega_{r,1} + \mathcal{O}(\epsilon^2)$$

$$p = p_o + \epsilon p_1 + \mathcal{O}(\epsilon^2)$$

The notation $\Omega_{r,i}$ represents the i -th order of the ϵ term. If we apply this perturbation to equation (4.15) and take the leading order we get

$$\frac{1}{r} \frac{\partial}{\partial r} \left(r \frac{\partial \Omega_{z,0}}{\partial r} \right) = 0 \quad (4.20)$$

Solving (4.20) we obtain,

$$\Omega_{z,0} = 0. \quad (4.21)$$

Given (4.21), the leading order of (4.13) becomes

$$\frac{1}{r} \frac{\partial}{\partial r} \left(r \frac{\partial (r \Omega_{r,0})}{\partial r} \right) - \frac{\Omega_{r,0}}{r^2} + \frac{1}{1-2\nu} \frac{\partial}{\partial r} \left(\frac{1}{r} \frac{\partial (r \Omega_{r,0})}{\partial r} \right) = 0$$

Solving this equation we get that

$$\Omega_{r,0} = c_1(z)r + \frac{c_2(z)}{r} \quad (4.22)$$

Combining (4.16) with these values of $\Omega_{z,0}$ and $\Omega_{r,0}$ and the boundary conditions (4.19) we obtain

$$\frac{1}{\eta} \left[(1-\nu) \left(c_1 - \frac{c_2}{r^2} \right) + \nu \left(c_1 + \frac{c_2}{r^2} \right) \right] \Big|_{r=a} = p_0 \Big|_{r=a} \quad (4.23)$$

and

$$\frac{\partial \sigma_r}{\partial r} \Big|_{r=1} = \frac{1}{\eta} [(1-\nu)(2c_2 - \nu 2c_2)] = 0 \quad (4.24)$$

It follows that from (4.24), we find that $c_2 = 0$ which tells us from (4.23) that $c_1 = \eta p_0 \Big|_{r=a}$. Therefore plugging everything into equation (4.22) we get that:

$$\Omega_{r,0}(r = a_0, z) = \eta p_0 a_0 \quad (4.25)$$

4.3.2 First-Order Analysis

From equation (4.13) focusing on the second highest order, thus $O(\epsilon)$, we get that:

$$\frac{1}{r} \frac{\partial}{\partial r} \left(r \frac{\partial(r\Omega_{r_1})}{\partial r} \right) - \frac{\Omega_{r_1}}{r^2} + \frac{1}{1-2\nu} \frac{\partial}{\partial r} \left(\frac{1}{r} \frac{\partial(r\Omega_{r_1})}{\partial r} \right) = 0$$

Solving this equation we get that

$$\Omega_{r,1} = c_1(z)r + \frac{c_2(z)}{r} \tag{4.26}$$

and just as before we get

$$\Omega_{r,1}(r, z) = \eta p_1 a_0 \tag{4.27}$$

Chapter 5

Particle Concentration in the Channel

Another important phenomena that affects the shape of the channel in the filtration process is the deposition of particles to the membrane channel wall.

5.1 Governing Equations

The transport of particles in the flow occurs due to the advection via fluid velocity and diffusion of the particles due to the gradient of the particle's concentration. Using the mass balance, the governing equation is:

$$\frac{\partial c}{\partial t} + \nabla \cdot \mathbf{Q}_c = 0, \quad \mathbf{Q}_c = -\Xi \nabla c + \mathbf{u}c, \quad (5.1)$$

where c is the particle concentration, \mathbf{Q}_c is the flux of particles, Ξ is the diffusion coefficient.

The concentration of the particles at the inlet of the channel is c_0 and at the end of the channel we considered the zero gradient concentration for the particles [21]. In addition, the particles are deposited on the wall, so there is a negative flux at the wall. Therefore, the boundary conditions are:

$$c|_{z=0} = c_0, \quad \frac{\partial c}{\partial z}|_{z=L} = 0, \quad \mathbf{Q}_c \cdot \mathbf{n}|_{r=a} = \alpha_1 c|_{r=a} \quad (5.2)$$

which α_1 is the stickiness coefficient of particles.

Timescale of the deposition process is much bigger than the flow, so we can assume quasi static assumption and consider that c is not function of time. Using the continuity equation and no slip boundary condition, the equations (5.1) and (5.2) reduces to the following equation in the cylindrical coordinate system:

$$\Xi \left(\frac{1}{r} \frac{\partial}{\partial r} \left(r \frac{\partial c}{\partial r} + \frac{1}{r^2} \frac{\partial^2 c}{\partial \theta^2} + \frac{\partial^2 c}{\partial z^2} \right) \right) = u \frac{\partial c}{\partial r} + \frac{v}{r} \frac{\partial c}{\partial \theta} + w \frac{\partial c}{\partial z} \quad (5.3)$$

$$- \Xi \left[\frac{\partial c}{\partial r} - \frac{1}{r^2} \frac{\partial c}{\partial \theta} \frac{\partial a}{\partial \theta} + \frac{\partial c}{\partial z} \frac{\partial a}{\partial z} \right] = \alpha_1 c|_{r=a} \quad (5.4)$$

5.2 Scaling and Non-dimensionalization

Using the scaling for the concentration as $c = c_0 \hat{c}$, which \hat{c} is the non-dimensionalized concentration, and other scaling constants are as defined in (2.15). Dropping $\hat{}$ symbol, for the non-dimensionalized parameters, the equations (5.3) and (5.4) reduce to:

$$\frac{1}{\epsilon Pe} \left[\frac{1}{r} \frac{\partial}{\partial r} \left(r \frac{\partial c}{\partial r} \right) + \frac{1}{r^2} \frac{\partial^2 c}{\partial \theta^2} + \epsilon^2 \frac{\partial^2 c}{\partial z^2} \right] = u \frac{\partial c}{\partial r} + \frac{v}{r} \frac{\partial c}{\partial \theta} + w \frac{\partial c}{\partial z}, \quad (5.5)$$

$$c|_{z=0} = 1, \quad \frac{\partial c}{\partial z}|_{z=1} = 0, \quad \frac{-1}{\epsilon Pe} \left[\frac{\partial c}{\partial r} - \frac{1}{r^2} \frac{\partial c}{\partial \theta} \frac{\partial a}{\partial \theta} + \epsilon^2 \frac{\partial c}{\partial z} \frac{\partial a}{\partial z} \right] = \alpha c|_{r=a}. \quad (5.6)$$

which $Pe = \frac{Q_i}{\pi \Xi R}$ and $\alpha = \frac{\pi \alpha_1 LR}{Q_i}$.

5.3 Asymptotic Analysis

Let $x = x_0 + \epsilon x_1 + \epsilon^2 x_2 + \dots$ where $x \in \{c, u, v, w\}$ and $a = a_0 + \epsilon a_1(\theta, z)$, substituting in equations (5.5) and (5.6), the governing equations and boundary conditions for orders $\mathcal{O}(\frac{1}{\epsilon})$, $\mathcal{O}(1)$ and $\mathcal{O}(\epsilon)$ are derived and solved below.

5.3.1 Leading Order Analysis

The leading order in equations (5.5) and (5.6) is $\mathcal{O}\left(\frac{1}{\epsilon}\right)$. Collecting all the terms with order of $\mathcal{O}\left(\frac{1}{\epsilon}\right)$, the governing equation and boundary conditions for the leading order are:

$$\frac{1}{r} \frac{\partial}{\partial r} \left(r \frac{\partial c_0}{\partial r} \right) + \frac{1}{r^2} \frac{\partial^2 c_0}{\partial \theta^2} = 0, \quad (5.7)$$

$$c_0|_{z=0} = 1, \quad \frac{\partial c_0}{\partial z}|_{z=1} = 0, \quad \frac{\partial c_0}{\partial r}|_{r=a_0} = 0. \quad (5.8)$$

For the channel wall configuration (2.25), the particle will be independent of θ in the leading order, so (5.7) reduces to:

$$\frac{\partial}{\partial r} \left(r \frac{\partial c_0}{\partial r} \right) = 0 \Rightarrow \frac{\partial c_0}{\partial r} = \text{const.} \quad (5.9)$$

Using boundary condition (5.8), we conclude that the constant value is zero and c_0 is not a function of r , then:

$$c_0 = c_0(z). \quad (5.10)$$

5.3.2 First-Order Analysis

The next term in the governing equations and boundary conditions is $\mathcal{O}(1)$. Collecting the terms with $\mathcal{O}(1)$, we have:

$$\frac{1}{Pe} \left[\frac{1}{r} \frac{\partial}{\partial r} \left(r \frac{\partial c_1}{\partial r} \right) + \frac{1}{r^2} \frac{\partial^2 c_1}{\partial \theta^2} \right] = w_0 \frac{dc_0}{dz}, \quad (5.11)$$

$$c_1|_{z=0} = 0, \quad \frac{\partial c_1}{\partial z}|_{z=1} = 0, \quad \frac{-1}{Pe} \frac{\partial c_1}{\partial r}|_{r=a_0} = \alpha c_0|_{r=a_0}. \quad (5.12)$$

In the above equation, there are two unknowns c_0 and c_1 . To reduce the number of the unknowns, we integrate the whole the equation with $\int_0^{2\pi} \int_0^{a_0} \cdot r dr d\theta$, then we can use the third part of equation (5.12) to relate $\frac{\partial c_1}{\partial r}$ to c_0 at $r = a_0$ and as c_0 is not function of r , then $c_0|_{r=a_0}(z) = c_0(z)$. Moreover, the second term in the left hand side of the equation (5.11) is zero due to the periodicity of $\frac{\partial c_1}{\partial \theta}$ at $\theta = 0$ and 2π . Then, the final differential

equation for c_0 after substituting w_0 using (2.35) is:

$$\frac{\partial c_0}{\partial z} = -2\alpha a_0 c_0 \Rightarrow c_0(z) = e^{-2\alpha a_0 z}, \quad (5.13)$$

which equation (5.8) is used to compute the integration constant.

5.3.3 Second-Order Analysis

To compute c_1 , we need to go one order further. The next term in the governing equations and boundary conditions is $\mathcal{O}(\epsilon)$. Collecting the terms with $\mathcal{O}(\epsilon)$ and using the result of the previous part (5.13) and (2.34), we have:

$$\frac{1}{Pe} \left[\frac{1}{r} \frac{\partial}{\partial r} \left(r \frac{\partial c_2}{\partial r} \right) + \frac{1}{r^2} \frac{\partial^2 c_2}{\partial \theta^2} + \frac{\partial^2 c_0}{\partial z^2} \right] = w_0 \frac{\partial c_1}{\partial z} + w_1 \frac{\partial c_0}{\partial z}, \quad (5.14)$$

$$\frac{-1}{Pe} \left[a_1 \frac{\partial^2 c_1}{\partial r^2} + \frac{\partial c_2}{\partial r} - \frac{1}{r^2} \frac{\partial c_1}{\partial \theta} \frac{\partial a_1}{\partial \theta} \right] = \alpha c_1|_{r=a_0}. \quad (5.15)$$

Similar to the previous part, we take the integral of the equation and use (5.15) to get an equation for c_1 which leads us to:

$$a_0 \int_0^{2\pi} \left\{ -\frac{1}{Pe} \left[a_1 \frac{\partial^2 c_1}{\partial r^2} - \frac{1}{r^2} \frac{\partial c_1}{\partial \theta} \frac{\partial a_1}{\partial \theta} \right] - \alpha c_1 \right\}_{r=a_0} d\theta + \frac{4\alpha^2 \pi}{Pe} a_0^2 e^{-2\alpha a_0 z} = \frac{2}{a_0^4} \int_0^{2\pi} \int_0^{a_0} \frac{\partial c_1}{\partial z} (a_0^2 - r^2) r dr d\theta. \quad (5.16)$$

We assume that c_1 is only function of z , so the above equation is simplified and using the second part in the boundary condition of (5.12), the solution for c_1 is:

$$c_1(z) = \frac{4\alpha^2 a_0^4}{Pe} z e^{-2\alpha a_0 z} \quad (5.17)$$

5.4 Final solution

Putting two first orders of c together from equations (5.13) and (5.17), the asymptotic solution for particle concentration is:

$$c = e^{-2\alpha a_0 z} + \frac{4\alpha^2 a_0^4}{Pe} z e^{-2\alpha a_0 z} \epsilon + \mathcal{O}(\epsilon^2) \quad (5.18)$$

Chapter 6

Results

In this section, we present some results simulating erosion and elasticity.

6.1 Channel with active erosion:

The figure below shows a channel with an initial radius of $a_0 = 0.6$, at different times.

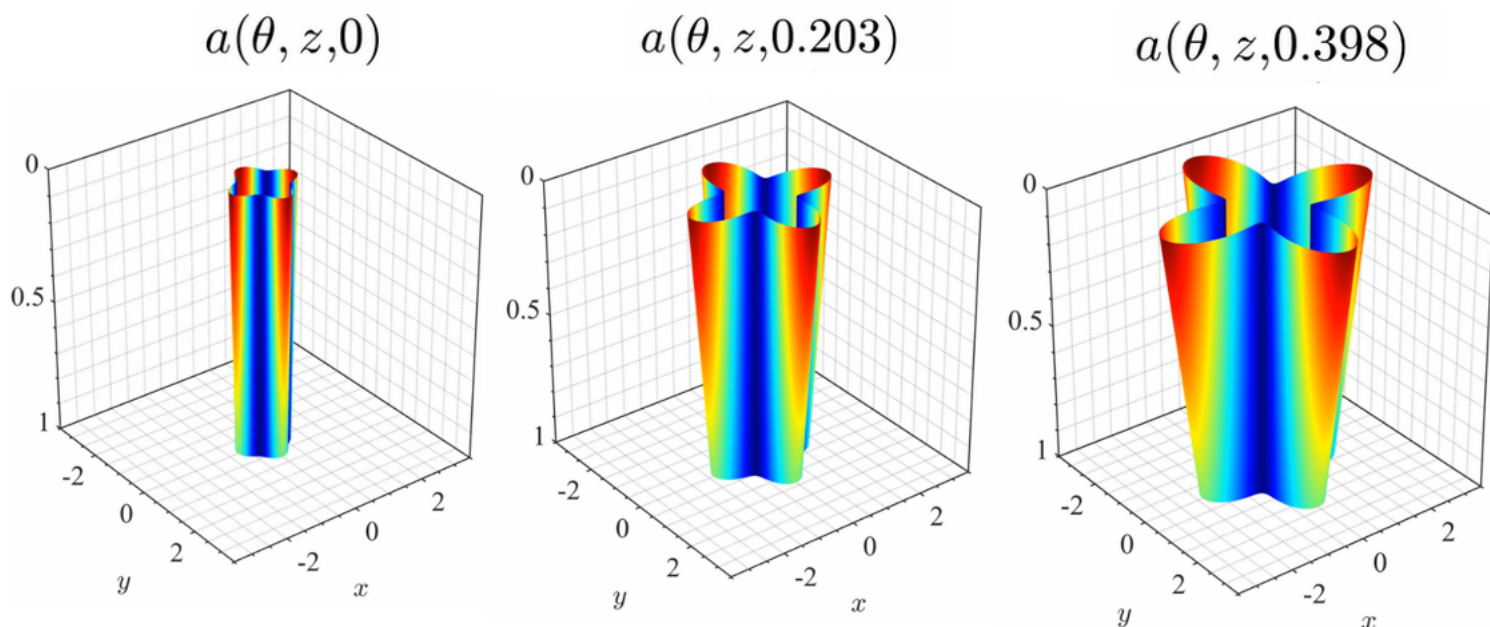


Figure 6.1: Erosion over time. Parameters include $n = 4$, $\lambda = 0.1$, $\Upsilon(z, 0) = 2 - z$, $\Lambda(z, 0) = 2 - z$, $a_0(0) = 0.6$ and $n = 4$.

Figures 6.2 and 6.3 show the effect of a 0.1 increase on λ .

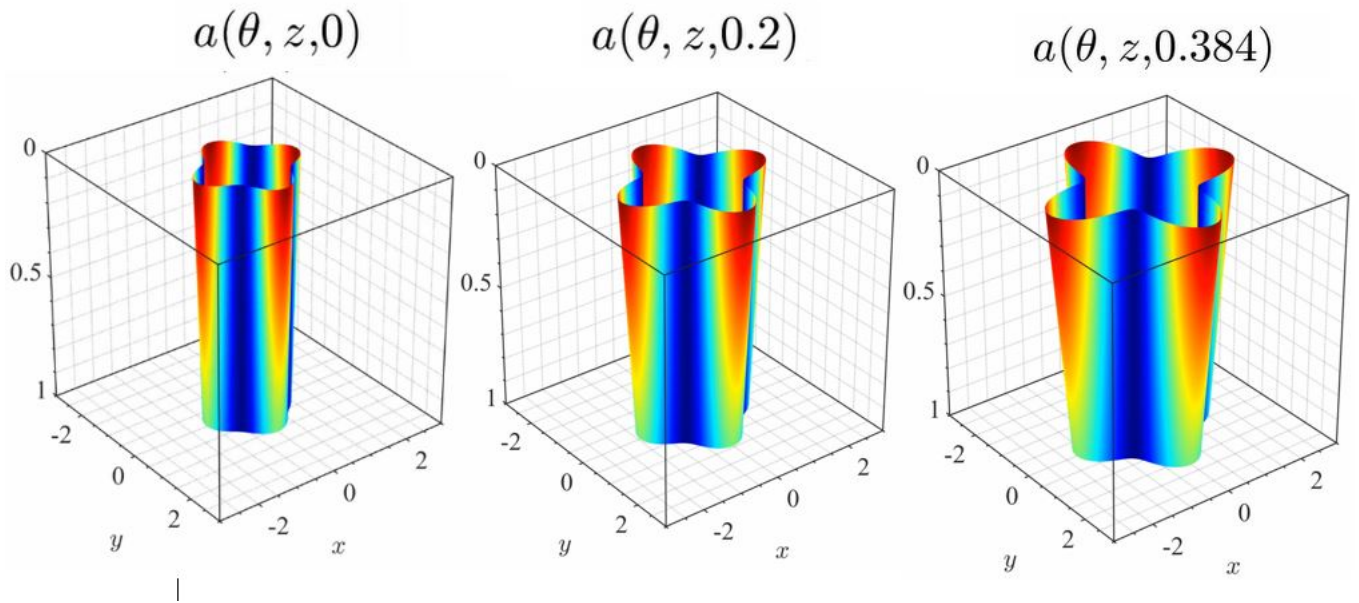


Figure 6.2: Erosion over time. Parameters include $n = 5$, $\lambda = 0.2$, $\Upsilon(z, 0) = 2 - z$, $\Lambda(z, 0) = 2 - z$, $a_0(0) = 0.9$ and $n = 4$.

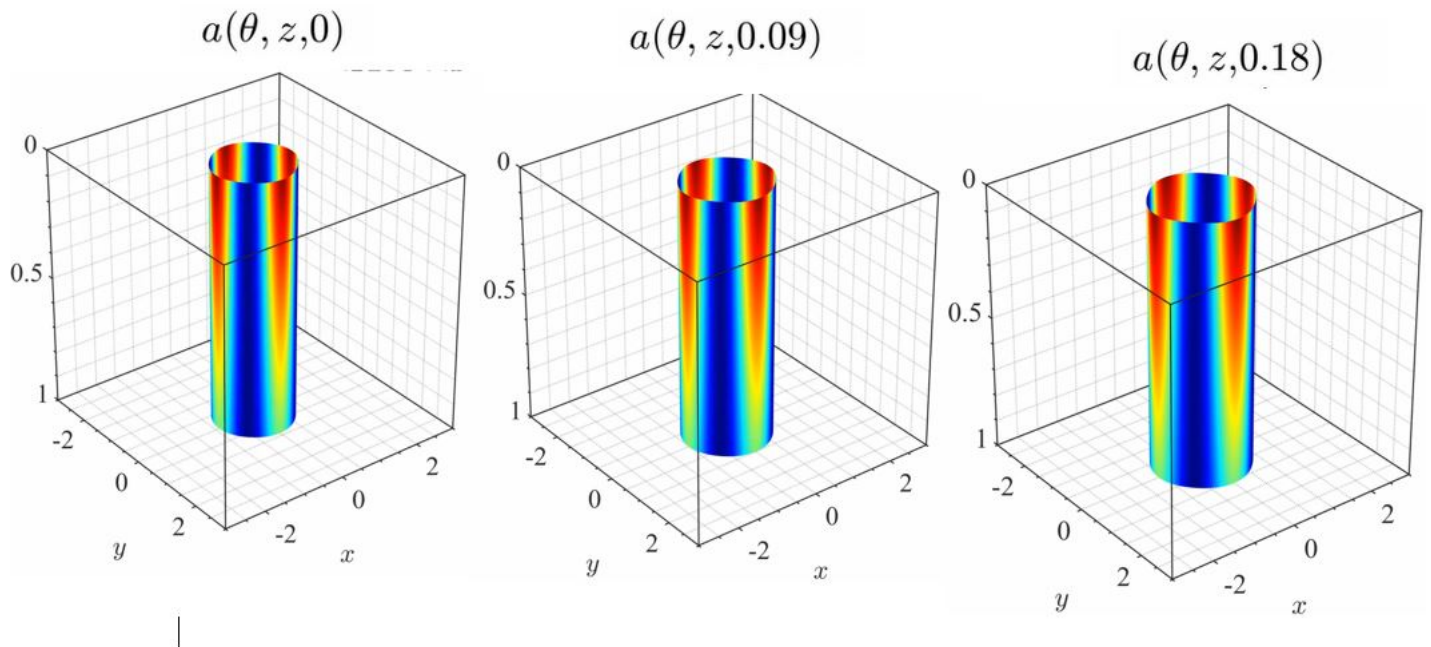


Figure 6.3: Erosion over time. Parameters include $n = 5$, $\lambda = 0.1$, $\Upsilon(z, 0) = 2 - z$, $\Lambda(z, 0) = 2 - z$, $a_0(0) = 0.9$ and $n = 4$.

Chapter 7

Conclusions

7.1 Conclusions/Extensions

We have presented a simplified mathematical model for the evolution of a channel to gain insight into the effect of erosion and elasticity on the channel morphology. The flow and elasticity were captured by the Stokes and Navier-Cauchy equations respectively, while the erosion was modelled by a law that accounted for the effects of the fluid shear stress at the increasing channel wall. Exploiting the geometrical features of a typical structure, namely a structure composed of a series of pores that are nearly cylindrical, allowed us to proceed via an asymptotic approach that led to a reduced system of four simple differential equations, while in many cases we were able to solve them analytically. The resulting equations were analyzed numerically and analytically for a typical erosion law, and an analytic expression was obtained when the erosion law is presented.

Chapter 8

Acknowledgements

We are especially thankful to the University of Delaware and the National Science Foundation for supporting us in this work. A special thank you to Dr. David A. Edwards for hosting GSMMC 2021.

Bibliography

- [1] Glen Bolton, Dan LaCasse, and Ralf Kuriyel. “Combined models of membrane fouling: development and application to microfiltration and ultrafiltration of biological fluids”. In: *Journal of Membrane Science* 277.1-2 (2006), pp. 75–84.
- [2] Zhengyi Chen et al. “Flow and fouling in elastic membrane filters with hierarchical branching pore morphology”. In: *In press at Physics of Fluids* (2021).
- [3] Mohit P Dalwadi, Ian M Griffiths, and Maria Bruna. “Understanding how porosity gradients can make a better filter using homogenization theory”. In: *Proceedings of the Royal Society A: Mathematical, Physical and Engineering Sciences* 471.2182 (2015), p. 20150464.
- [4] Chase Duclos-Orsello, Weiyi Li, and Chia-Chi Ho. “A three mechanism model to describe fouling of microfiltration membranes”. In: *Journal of Membrane Science* 280.1-2 (2006), pp. 856–866.
- [5] Irving Fatt. “The network model of porous media”. In: *Transactions of the AIME* 207.01 (1956), pp. 144–181.
- [6] Robin Fell et al. “Time for development of internal erosion and piping in embankment dams”. In: *Journal of geotechnical and geoenvironmental engineering* 129.4 (2003), pp. 307–314.
- [7] X Romam Fernández et al. “Experimental and analytical modeling of the filtration mechanisms of a paper stack candle filter”. In: *Chemical Engineering Research and Design* 89.12 (2011), pp. 2776–2784.

- [8] IM Griffiths, A Kumar, and PS Stewart. “Designing asymmetric multilayered membrane filters with improved performance”. In: *Journal of membrane science* 511 (2016), pp. 108–118.
- [9] IMk Griffiths, A Kumar, and PS Stewart. “A combined network model for membrane fouling”. In: *Journal of colloid and interface science* 432 (2014), pp. 10–18.
- [10] Syunsuke Ikeda, Gary Parker, and Kenji Sawai. “Bend theory of river meanders. Part 1. Linear development”. In: *Journal of Fluid Mechanics* 112 (1981), pp. 363–377.
- [11] Eiji Iritani. “A review on modeling of pore-blocking behaviors of membranes during pressurized membrane filtration”. In: *Drying technology* 31.2 (2013), pp. 146–162.
- [12] Robin Jäger, Miller Mendoza, and Hans Jürgen Herrmann. “Channelization in porous media driven by erosion and deposition”. In: *Physical Review E* 95.1 (2017), p. 013110.
- [13] Elizabeth Koch. *Multi-layer filter*. US Patent 4,483,771. Nov. 1984.
- [14] M Nicholas J Moore. “Riemann-Hilbert Problems for the Shapes Formed by Bodies Dissolving, Melting, and Eroding in Fluid Flows”. In: *Communications on Pure and Applied Mathematics* 70.9 (2017), pp. 1810–1831.
- [15] Matthew NJ Moore et al. “Self-similar evolution of a body eroding in a fluid flow”. In: *Physics of Fluids* 25.11 (2013), p. 116602.
- [16] Leif Ristroph et al. “Sculpting of an erodible body by flowing water”. In: *Proceedings of the National Academy of Sciences* 109.48 (2012), pp. 19606–19609.
- [17] Pejman Sanaei and Linda J Cummings. “Membrane filtration with complex branching pore morphology”. In: *Physical Review Fluids* 3.9 (2018), p. 094305.
- [18] Pejman Sanaei and Linda J Cummings. “Membrane filtration with multiple fouling mechanisms”. In: *Physical Review Fluids* 4.12 (2019), p. 124301.
- [19] SA Schumm and HR Khan. “Experimental study of channel patterns”. In: *Geological Society of America Bulletin* 83.6 (1972), pp. 1755–1770.
- [20] Yixuan Sun et al. “Modeling and design optimization for pleated membrane filters”. In: *Physical Review Fluids* 5.4 (2020), p. 044306.

- [21] Geoffrey Ingram Taylor. “Dispersion of soluble matter in solvent flowing slowly through a tube”. In: *Proceedings of the Royal Society of London. Series A. Mathematical and Physical Sciences* 219.1137 (1953), pp. 186–203.
- [22] C. Truesdell and W. Noll. “The Non-Linear Field Theories of Mechanics”. In: 2nd (1992).
- [23] A Wesley Ward. “Yardangs on Mars: Evidence of recent wind erosion”. In: *Journal of Geophysical Research: Solid Earth* 84.B14 (1979), pp. 8147–8166.
- [24] Kyunghwan Yoon et al. “High flux ultrafiltration membranes based on electrospun nanofibrous PAN scaffolds and chitosan coating”. In: *Polymer* 47.7 (2006), pp. 2434–2441.